JACS
JOURNAL OF THE AMERICAN CHEMICAL SOCIETY

Communication

Vapor-Phase Strategy to Pillaring of Two-Dimensional Zeolite

Lu Wei, Kechen Song, Wei Wu, Scott Holdren, Guanghui Zhu, Emily Schulman, Wenjin Shang, Huiyong Chen, Michael R. Zachariah, and Dongxia Liu

J. Am. Chem. Soc., **Just Accepted Manuscript** • Publication Date (Web): 22 May 2019

Just Accepted

is published by the American Chemical Society. 1155 Sixteenth Street N.W., Washington, DC 20036

Vapor-Phase Strategy to Pillaring of Two-Dimensional Zeolite

Lu Wei[1,2], Kechen Song[2,3], Wei Wu[2], Scott Holdren[4], Guanghui Zhu[5], Emily Shulman[2], Wenjin Shang[6], Huiyong Chen[6], Michael R. Zachariah[4±] and Dongxia Liu[2*]

1.College of Materials Science and Engineering, Beijing University of Technology, Beijing 100124, PR China

2.Department of Chemical and Biomolecular Engineering, University of Maryland, College Park, MD, 20742, USA

3.School of Chemical and Environmental Engineering, China University of Mining and Technology, Beijing, 100083, China

4.Department of Chemistry and Biochemistry, University of Maryland, College Park, MD, 20742, USA

5.School of Chemical and Biomolecular Engineering, Georgia Institute of Technology, Atlanta, 30332, USA

6.School of Chemical Engineering, Northwest University, Xi'an, Shanxi, 710069, China

± current address: Department of Chemical and Environmental Engineering, University of California, Riverside mrz@engr.ucr.edu

Supporting Information Placeholder

ABSTRACT: Two-dimensional (2D) layered zeolites are new forms of 3D zeolite frameworks. They can be pillared to form more open porous structures with increased access for reactants that are too big for the micropores of zeolites. The current pillaring procedure, however, requires intercalation of pillaring precursors by dispersing 2D zeolite in an alkoxide liquid and hydrolizing entrapped alkoxide to form inorganic oxide pillars in an aqueous alkaline solution. Both steps use excess solvents, generate significant waste, and require multiple synthesis and separation steps. Here we report a vapor phase pillarization (VPP) process to produce pillared zeolites from 2D layered zeolite structures. The VPP process has ~100% efficiency of alkoxide usage in the intercalation step, requires less (and, in some cases, zero) water addition in the hydrolysis step, does not require separation for product recovery, and generates no liquid waste. Furthermore, synthesis of pillared zeolites via the VPP process can be accomplished within a single apparatus with one-time operation. The pillared zeolite prepared by the VPP method preserved zeolitic layered structure as well as acidity and showed enhancement in catalytic alkylation of mesitylene with benzyl alcohol compared to 2D layered zeolite without pillarization treatment.

Two-dimensional (2D) layered zeolites contain a stack of microporous crystalline aluminosilicate sheets, each of which has one or a fraction of the unit-cell thickness, equivalent to a few nanometers.[1-4] The atoms within the zeolitic layers are connected by strong covalent bonds, while the contiguous zeolitic layers are linked by van der Waals forces, hydrogen bonds or ionic interactions (i.e. interaction between terminal silanol groups and charged structure directing agents).[5-7] The interlayer interactions in 2D zeolites determine the potential for a variety of structural and chemical modifications within the interlayer space between adjacent zeolitic layers with preservation of the original layer integrity. Therefore, 2D zeolite materials can be considered as host scaffolds that can expand and/or extend via structural, topotactic and compositional modifications to form novel and diverse structures.

Two basic chemical processes, exfoliation[8-14] and pillarization[15-25], have been used to modify 2D zeolites into diverse structures. The exfoliation process separates the stack of 2D zeolite nanosheets into self-standing independent entities by breaking down the interlayer interactions. The exfoliated zeolite nanosheets can be used as a base material for the fabrication of membranes[26-28] or used directly as hierarchical catalysts[29-31]. Rather than breaking down the stack of 2D zeolites in the exfoliation process, the pillarization process transforms the 2D zeolites into hierarchical materials with the retention of the stacked layer structure. The pillarization often involves subsequent expansion of interlayer space by swelling with long chain polar organic molecules, intercalation of the swollen materials in an alkoxide liquid, hydrolysis of entrapped alkoxide in an aqueous alkaline solution, and removal of organics as well as transformation of alkoxide liquid into permanent oxide pillars between zeolitic layers by calcination.[16-19, 22] The current pillaring procedure requires multiple discrete steps, uses excess solvents in both intercalation and hydrolysis treatments, and generates waste.

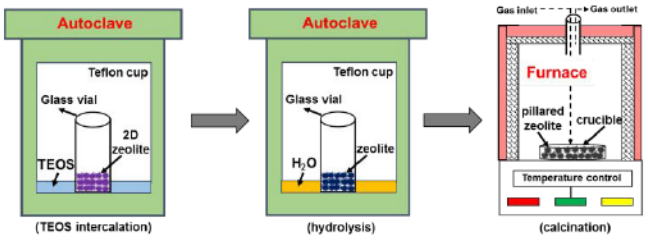

Figure 1. Schematic of the formation of pillared zeolite from 2D layered zeolite in the VPP process.

Here, we report on a vapor phase pillarization (VPP) process to produce pillared zeolites from 2D layered zeolite materials. The experimental set-up (Figure 1) is similar to that used in steam-assisted zeolite crystallization[32-33] in a Teflon-lined autoclave. A glass vial containing 2D layered zeolite is placed in the Teflon cup. The pillaring precursor (i.e., liquid alkoxide) is dropped into the Teflon cup and separated from the 2D layered zeolite by the glass container. After heating the autoclave to evaporate alkoxide for intercalation, the same set-up is used to evaporate water for hydrolysis of intercalated alkoxide (Section S1). The mass ratios of alkoxide/zeolite and water/zeolite are controlled as 0.5 and 10 in the intercalation and hydrolysis steps, respectively. The 2D layered zeolite is calcined in a furnace to form the pillared zeolite. In comparison to pillarization of 2D layered zeolites in liquid solvent/solution reported previously[16-19, 22], the VPP method requires up to ~10 times less alkoxide in the intercalation step, uses less (and even zero, to be discussed below) water addition in the hydrolysis step, does not require product recovery from the liquid solvent/solution, and generates no liquid waste.

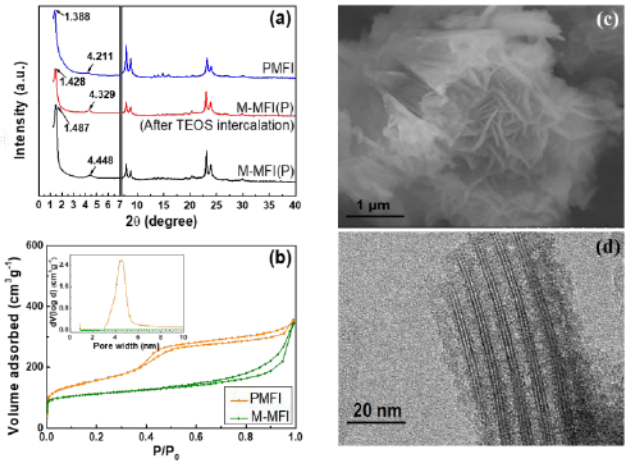

Figure 2. Characterization of PMFI formed in VPP process. (a) XRD patterns M-MFI(P) at different synthesis stages and PMFI, and (b) N_2 isotherm of PMFI and M-MFI samples. (c) and (d) are SEM and TEM images of PMFI zeolite. (VPP conditions: 0.1 g M-MFI(P), 0.05 g TEOS, 1 g H_2O, intercalation at 423 K for 24 h, hydrolysis at 353 K for 24 h.)

As a prominent representative of 2D layered zeolite, multilamellar MFI (M-MFI)[31], synthesized by hydrothermal crystallization of a synthetic gel comprising of zeolite precursor materials and a diquanternary ammonium template (Section S1.2), was used as the precursor (M-MFI(P)) to form pillared MFI (PMFI) zeolite using the VPP process. Tetraethyl orthosilicate (TEOS) and deionized water (DI H_2O) were used in the intercalation and hydrolysis steps, respectively, to form silica (SiO_2) pillars in PMFI. Figure 2(a) shows the XRD patterns of M-MFI(P) and M-MFI(P) after TEOS intercalation and PMFI synthesized using the VPP process. The characteristic diffraction peaks of the MFI structure[31] in the wide-angle range in Figure 1(a) suggest that crystalline MFI framework was retained in the VPP process. The low-angle diffraction peaks[22, 34] indicate preservation of the 2D layered structure in pillarization. The N_2 isotherms and pore size distributions (Figure 2(b)) show that PMFI has much higher surface area and mesoporosity than M-MFI prepared from direct calcination of M-MFI(P). The PMFI prepared with the VPP process preserves the nanosheet aggregate morphology of M-MFI(P)[31] (scanning electron microscopy (SEM) image in Figure 2(c)). The ordering of zeolitic nanosheets is clearly visualized by transmission electron microscopy (TEM) of PMFI in Figure 2(d).

To explore the influence of TEOS quantity on formation of PMFI in the VPP process, the mass ratio of TEOS to M-MFI(P) (i.e., TEOS/M-MFI(P)) was varied from 0.05 to 3.75 (Section S2.1). The bulk morphology of the M-MFI(P) sample after the intercalation step transformed from a white, dry powder into a pale yellow gel with increasing TEOS usage (Figure S1). The TEOS liquid in the Teflon cup had disappeared when the TEOS/M-MFI(P) ratio was below 0.5, while TEOS liquid droplets appeared on the walls of both the Teflon cup and glass vial with TEOS/M-MFI(P) ratios of 1.00 and 3.75. The appearance of a "bump" peak (2θ ~ 13.5°) in the wide-angle XRD (Figure S2) of PMFI synthesized with a TEOS/M-MFI(P) ratio of 1.00 and 3.75 indicates the emergence of amorphous material from excess TEOS quantity. The disappearance of diffraction peaks in the low-angle XRD of PMFI synthesized with a TEOS/M-MFI(P) ratio of 0.05 suggests collapse of the layered zeolitic structure since the SiO_2 pillars formed using TEOS concentrations were insufficient to maintain the layered structure integrity upon organic template removal via calcination. The TEOS/M-MFI(P) ratio of 0.50 and 0.10 produced PMFI with high crystallinity, ordering of zeolitic nanosheet layers and high mesoporosity (isotherm data in Figure S3 and Table S1). The intercalation temperature did not influence PMFI formation significantly under investigated conditions. The XRD patterns (Figure S4) and N_2 isotherms (Figure S5) of PMFI synthesized at intercalation temperatures of 363, 383, 403 and 423 K with the VPP process are very similar.

The effects of water in the hydrolysis step on PMFI formation were examined by varying the mass ratio of water to M-MFI(P) (H_2O/M-MFI(P)) from 10 to 0 in the VPP process. In all cases, PMFI was synthesized successfully, as confirmed by both XRD (Figure S6) and N_2 isotherm (Figure S7) data. The formation of PMFI can be completed even with no water added, which is unexpected since water is considered a required material for TEOS hydrolysis to form the pillars[35]. However, since the M-MFI(P) was dried in a convective oven at 343 K for 12 h after the hydrothermal crystallization, it is likely that adsorbed water remained in the porous zeolite structures. Alkali ions and diquanternary ammonium template molecules trapped in M-MFI(P) from the hydrothermal synthesis provide sufficient basicity for TEOS hydrolysis, since a pH of 8 (by NaOH solution) is commonly used in the liquid-phase pillarization in previous methods[16-19, 22]. The thermogravimetric analysis (TGA) (Figure S8) shows that M-MFI(P) contains ~16% H_2O, which closely corresponds to the water amount required for complete hydrolysis of TEOS in the intercalation step (calculation details see Section S2.3). This is consistent with the fact that the pillared structure was unable to form when the M-MFI(P) sample was dried in a vacuum oven at 393 K for 12 h (absence of low-angle XRD peaks in Figure S9).

The zero water addition in the VPP process suggests an option to further simplify the zeolite pillarization protocol. In this case, we eliminated the TEOS hydrolysis step and integrated TEOS intercalation and zeolite calcination steps into one apparatus to realize a one-time operation for the synthesis of PMFI zeolite. In the new VPP protocol, the apparatus is a furnace containing a quartz "U"-shaped tube (Figure 3, for details refer to Section S1.3). The 2D layered zeolite is added into the "bulb" region of the quartz tube from one opening, while liquid alkoxide solvent is dropped from the other opening. A quartz frit isolates the 2D layered zeolite from direct contact with alkoxide liquid before the VPP process starts. After operating the furnace according to the temperature profile shown in Figure 3, PMFI (confirmed by XRD (Figure S10) and N_2 isotherm (Figure S11) in the Supporting Information) was formed along with complete TEOS consumption. Therefore, the entire VPP process only requires a single apparatus and one-time operation and does not require further separation for product recovery or generate liquid waste; this process can achieve ~100% efficiency in zeolite and TEOS utilization for the formation of pillared zeolite.

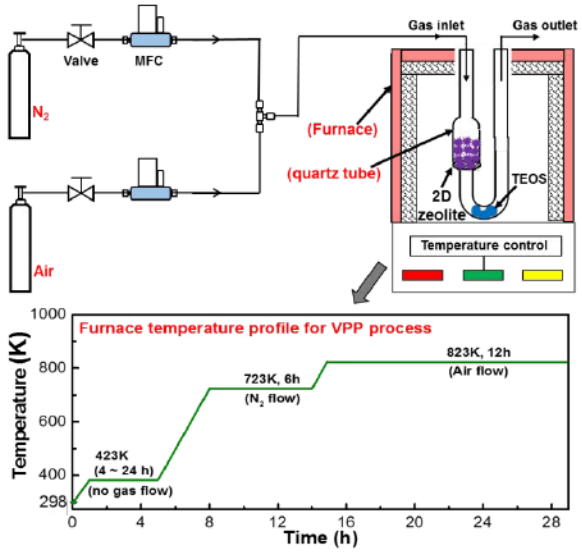

Figure 3. Experimental configuration and temperature profile for VPP of 2D zeolite in one unit under one-time operation.

The composition, acidity and catalytic performance of PMFI synthesized from the VPP process was characterized. The silicon (Si) and aluminum (Al) contents of PMFI are nearly identical to those calculated using M-MFI(P) and TEOS quantities, assuming all TEOS was consumed during the transformation into SiO_2 pillars (Table S2). This confirms the complete consumption of alkoxide liquid in the VPP process, which is consistent with visual observation. FTIR spectra of the OH-stretching mode (ν(OH)) and adsorbed pyridine in PMFI and M-MFI (Figure 4(a-b)) were recorded to understand their acidity properties. In Figure 4(a), three peaks centered around 3739 cm^{-1}, 3674 cm^{-1} and 3614 cm^{-1} are associated with terminal silanol (Si-OH) groups, extra-framework Al-OH species, and Brønsted acid site (Si-O(H)-Al) groups[36-38], respectively, on both M-MFI and PMFI. Both samples showed comparable characteristic peaks for Brønsted (1545 cm^{-1}) and Lewis (1450 cm^{-1}) acid sites[36, 38-39] in the FTIR spectra of adsorbed pyridine (Figure 4(b)). These results indicate acidity properties of the 2D zeolites were not destroyed during the VPP process. Solid state NMR (Figure 4(c)) was employed to investigate the local bonding environment of Si and Al species in the PMFI zeolite by recording the ^{29}Si single pulse (SP) and ^{27}Al NMR spectra. In the top panel, the peak (-113 ppm) corresponding to the crystallographically nonequivalent Q^4 tetrahedral sites (Q^n stands for $X_{4-n}Si[OSi]_n$)[34, 40-41] is much stronger than that of Q^3 sites (-103 ppm) arising from the silanol groups. In the bottom panel, the peak at 55 ppm is due to the tetrahedrally coordinated framework aluminum (Al_F), whereas the peak around 0 ppm is due to an octahedral coordination typical of extra-framework Al (Al_{EF}).[19, 31] The NMR spectrum of PMFI prepared via the VPP process is similar to that of M-MFI[31] and PMFI synthesized by the liquid phase pillarization method[34]. The catalytic conversion of benzyl alcohol in mesitylene, a reaction that requires mesoporosity in MFI to enable high activity[25, 42-44], shows that PMFI had higher benzyl alcohol conversion than M-MFI and conventional MFI (Figure 4(d), experimental details see Section S1.5), suggesting the successful formation of a pillared hierarchical zeolite structure for space-demanding catalytic reactions. The catalytic performance of PMFI prepared by the VPP process is comparable to that synthesized by the conventional liquid-phase pillarization approach (Figure S12)".

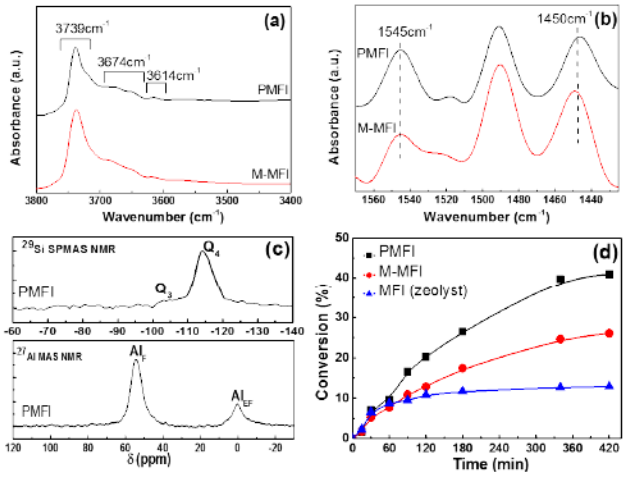

Figure 4. Acidity and catalytic performance of PMFI prepared by VPP process. (a) DRIFTS spectra, (b) FTIR spectra of adsorbed pyridine, (c) ^{29}Si (top panel) and ^{27}Al (bottom panel) MAS-NMR and (d) benzyl alcohol conversion of mesitylene, respectively.

In conclusion, we demonstrate that the pillarization of 2D layered zeolite can be accomplished by the VPP method that integrates three discrete operation steps (intercalation, hydrolysis and calcination, typically practiced in zeolite pillarization) into a single operation using only one apparatus. The VPP protocol has ~100% efficiency in usage of alkoxide liquid as well as zeolite materials and does not generate liquid waste. The pillared zeolite prepared using the VPP process has preserved the structural integrity (both framework crystallinity and ordering of zeolitic nanosheet layers), acidity and catalytic performance of the zeolite framework in comparison to 2D zeolite prepared using direct calcination. The VPP process is scalable, easy to operate, remarkably simple and highly efficient compared to the previous liquid-

phase pillarization method, which could pave a new avenue towards pillaring additional 2D zeolites and new types of layered materials.

ASSOCIATED CONTENT

Supporting Information

Experimental details for synthesis and characterization of M-MFI(P), M-MFI and PMFI; catalyst preparation for catalysis study and details in catalysis tests; additional XRD and N_2 isotherm and TGA analyses. This material is available free of charge via the Internet at http://pubs.acs.org.

AUTHOR INFORMATION

Corresponding Author

Prof. Dongxia Liu
Email: liud@umd.edu
Phone: (+1) 301-405-3522
Fax: (+1) 301-405-0523

Notes

The authors declare no competing financial interests.

ACKNOWLEDGMENT

Lu Wei and Kechen Song thanks for fellowship support from the China Scholarship Council. This work was supported by the US National Science Foundation (CBET-1706059). This work was supported as part of the Catalysis Center for Energy Innovation, an Energy Frontier Research Center funded by the U.S. Department of Energy, Office of Science, Office of Basic Energy Sciences, under Award No. DE-SC0001004. The authors acknowledge the support of the Maryland NanoCenter and its NispLab. The NispLab is supported in part by the NSF as a MRSEC Shared Experimental Facility.

REFERENCES

1. Díaz, U. Layered Materials with Catalytic Applications: Pillared and Delaminated Zeolites from MWW Precursors. ISRN Chemical Engineering. 2012, Article ID 537164.

2. Li, C.; Moliner, M.; Corma, A. Building Zeolites from Precrystallized Units: Nanoscale Architecture. Angew. Chem. Int. Ed., 2018, 57, 15330.

3. Přech, J.; Pizarro, P.; Serrano, D. P.; Čejka. From 3D to 2D zeolite catalytic materials. J. Chem. Soc. Rev. 2018, 47, 8263.

4. Roth, W. J.; Nachtigall, P.; Morris, R. E.; Čejka, J. Two-Dimensional Zeolites: Current Status and Perspectives. Chem. Rev. 2014, 114, 4807.

5. Marler, B.; Gies, H. Hydrous layer silicates as precursors for zeolites obtained through topotactic condensation: a review. Eur. J. Mineral. 2012, 24, 405.

6. Roth, W. J.; Dorset, D. L. The role of symmetry in building up zeolite frameworks from layered zeolite precursors having ferrierite and CAS layers. Struc. Chem. 2010, 21, 385.

7. Xu, L.; Sun, J. Recent Advances in the Synthesis and Application of Two-Dimensional Zeolites. Adv. Energy Mater. 2016, 6, 1600441.

8. Corma, A.; Fornes, V.; Pergher, S. B.; Maesen, T. L. M.; Buglass, J. G. Delaminated zeolite precursors as selective acidic catalysts. Nature. 1998, 396, 353.

9. Maheshwari, S.; Jordan, E.; Kumar, S.; Bates, F. S.; Penn, R. L.; Shantz, D. F.; Tsapatsis, M. Layer Structure Preservation during Swelling, Pillaring, and Exfoliation of a Zeolite Precursor. J. Am. Chem. Soc. 2008, 130, 1507.

10. Sabnis, S.; Tanna, V. A.; Li, C.; Zhu, J.; Vattipalli, V.; Nonnenmann, S. S.; Sheng, G.; Lai, Z.; Winter, H. H.; Fan, W. Exfoliation of two-dimensional zeolites in liquid polybutadienes. Chem. Commun. 2017, 53, 7011.

11. Gil, B.; Makowski, W.; Marszalek, B.; J. Roth, W.; Kubu, M.; Čejka, J.; Olejniczak, Z. High acidity unilamellar zeolite MCM-56 and its pillared and delaminated derivatives. Dalton Trans. 2014, 43, 10501.

12. Ogino, I.; Eilertsen, E. A.; Hwang, S.-J.; Rea, T.; Xie, D.; Ouyang, X.; Zones, S. I.; Katz, A. Heteroatom-Tolerant Delamination of Layered Zeolite Precursor Materials. Chem. Mater. 2013, 25, 1502.

13. Corma, A.; Diaz, U.; Domine, M. E.; Fornés, V. AlITQ-6 and TiITQ-6: Synthesis, Characterization, and Catalytic Activity. Angew. Chem. Int. Ed. 2000, 39, 1499.

14. Varoon, K.; Zhang, X.; Elyassi, B.; Brewer, D. D.; Gettel, M.; Kumar, S.; Lee, J. A.; Maheshwari, S.; Mittal, A.; Sung, C.-Y.; Cococcioni, M.; Francis, L. F.; McCormick, A. V.; Mkhoyan, K. A.; Tsapatsis, M. Dispersible Exfoliated Zeolite Nanosheets and Their Application as a Selective Membrane. Science. 2011, 334, 72.

15. Kosuge, K.; Tsunashima, A., New silica-pillared material prepared from the layered silicic acid of ilerite. New silica-pillared material prepared from the layered silicic acid of ilerite. J. Chem. Soc. Chem. Commun. 1995, 23, 2427.

16. Roth, W. J.; Kresge, C. T.; Vartuli, J. C.; Leonowicz, M. E.; Fung, A. S.; McCullen, S. B. in Studies in Surface Science and Catalysis, ed. Beyer, H. K.; Karge, H. G.; Kiricsi I.; Nagy, J. B. Inorganic MCM-36: TEOS pillaring from swollen MCM(P). 1995, 94, pp. 301.

17. Kresge, C. T.; Roth, W. J.; Simmons, K. G.; Vartuli, J. C. A method of preparing a pillared layered oxide material (Mobil Oil Corporation) WO Patent 92/011935, 1992.

18. Kresge, C. T.; Roth, W. J.; Simmons K. G.; Vartuli, J. C. Crystalline oxide material (Mobil Oil Corporation). US Patent 5,229,341, 1993.

19. Maheshwari, S.; Martínez, C.; Teresa Portilla, M.; Llopis, F. J.; Corma, A.; Tsapatsis, M. Influence of layer structure preservation on the catalytic properties of the pillared zeolite MCM-36. J. Catal. 2010, 272, 298.

20. Jin, F.; Chang, C.-C.; Yang, C.-W.; Lee, J.-F.; Jang, L.-Y.; Cheng, S. New mesoporous titanosilicate MCM-36 material synthesized by pillaring layered ERB-1 precursor. J. Mater. Chem. A. 2015, 3, 8715.

21. Roth, W. J.; Gil, B.; Mayoral, A.; Grzybek, J.; Korzeniowska, A.; Kubu, M.; Makowski, W.; Čejka, J.; Olejniczak, Z.; Mazur, M. Pillaring of layered zeolite precursors with ferrierite topology leading to unusual molecular sieves on the micro/mesoporous border. Dalton Trans. 2018, 47, 3029.

22. Na, K.; Choi, M.; Park, W.; Sakamoto, Y.; Terasaki, O.; Ryoo, R. Pillared MFI Zeolite Nanosheets of a Single-Unit-Cell Thickness. J. Am. Chem. Soc. 2010, 132, 4169.

23. Liu, B.; Wattanaprayoon, C.; Oh, S. C.; Emdadi, L.; Liu, D. Synthesis of Organic Pillared MFI Zeolite as Bifunctional Acid–Base Catalyst. Chem. Mater. 2015, 27, 1479.

24. Emdadi, L.; Tran, D. T.; Zhang, J.; Wu, W.; Song, H.; Gan, Q.; Liu, D. Synthesis of titanosilicate pillared MFI zeolite as an efficient photocatalyst. RSC Adv. 2017, 7, 3249.

25. Zhang, X.; Liu, D.; Xu, D.; Asahina, S.; Cychosz, K. A.; Agrawal, K. V.; Al Wahedi, Y.; Bhan, A.; Al Hashimi, S.; Terasaki, O.; Thommes, M.; Tsapatsis, M. Synthesis of Self-Pillared Zeolite Nanosheets by Repetitive Branching. Science. 2012, 336.

26. Agrawal, K. V.; Topuz, B.; Pham, T. C. T.; Nguyen, T. H.; Sauer, N.; Rangnekar, N.; Zhang, H.; Narasimharao, K.; Basahel, S. N.; Francis, L. F.; Macosko, C. W.; Al-Thabaiti, S.; Tsapatsis, M.; Yoon, K. B. Oriented MFI membranes by gel-less secondary growth of Sub-100 nm MFI-nanosheet seed layers, 2015, 27, 3243.

27. Zou, C.; Lin, L. C. Exploring the potential and design of zeolite nanosheets as pervaporation membranes for ethanol extraction. Chem. Commun. 2018, 54, 13200.

28. Zhang, H.; Xiao, Q.; Guo, X.; Li, N.; Kumar, P.; Rangnekar, N.; Jeon, M. Y.; Al-Thabaiti, S.; Narasimharao, K.; Basahel, S. N.; Topuz, B.; Onorato, F. J.; Macosko, C. W.; Mkhoyan, K. A.; Tsapatsis, M. Open-Pore Two-Dimensional MFI Zeolite Nanosheets for the Fabrication of Hydrocarbon-Isomer-Selective Membranes on Porous Polymer Supports. Angew. Chem. Int. Ed. 2016, 55, 7184.

29. Meng, L.; Zhu, X.; Hensen, E. J. M. Stable Fe/ZSM-5 Nanosheet Zeolite Catalysts for the Oxidation of Benzene to Phenol. ACS Catal. 2017, 7, 2709.

30. Jung, J.; Jo, C.; Cho, K.; Ryoo, R. Zeolite nanosheet of a single-pore thickness generated by a zeolite-structure-directing surfactant. J. Mater. Chem. 2012, 22, 4637.

31. Choi, M.; Na, K.; Kim, J.; Sakamoto, Y.; Terasaki, O.; Ryoo, R. Stable single-unit-cell nanosheets of zeolite MFI as active and long-lived catalysts. Nat. Mater. 2009, 461, 246.

32. Fan, W.; Snyder, M. A.; Kumar, S.; Lee, P.-S.; Yoo, W. C.; McCormick, A. V.; Lee Penn, R.; Stein, A.; Tsapatsis, M. Hierarchical nanofabrication of microporous crystals with ordered mesoporosity. Nat. Mater 2008, 7, 984.

33. Chen, H.; Wydra, J.; Zhang, X.; Lee, P.-S.; Wang, Z.; Fan, W.; Tsapatsis, M. Hydrothermal Synthesis of Zeolites with Three-Dimensionally Ordered Mesoporous-Imprinted Structure. J. Am. Chem. Soc. 2011, 133, 12390.

34. Liu, D.; Bhan, A.; Tsapatsis, M.; Al Hashimi, S. Catalytic Behavior of Brønsted Acid Sites in MWW and MFI Zeolites with Dual Meso- and Microporosity. ACS. Catal. 2011, 1, 7.

35. Innocenzi, P., The Sol to Gel Transition. Springer Briefs in Materials, Springer International Publishing, 2016, pp.7.

36. Busca, G. pectroscopic characterization of the acid properties of metal oxide catalysts. Catal. Today. 1998, 41, 191.

37. Jiang, M.; Karge, H. G. J. Chem. Soc. 1996, 92, 2641.

38. Trombetta, M.; Busca, G. On the Characterization of the External Acid Sites of Ferrierite and Other Zeolites: A Reply to Pieterse et al. J. Catal. 1999, 187, 521.

39. Bai, Y.; Wei, L.; Yang, M.; Chen, H.; Holdren, S.; Zhu, G.; Tran, D. T.; Yao, C.; Sun, R.; Pan, Y.; Liu, D. Three-step cascade over a single catalyst: synthesis of 5-(ethoxymethyl)furfural from glucose over a hierarchical lamellar multi-functional zeolite catalyst. J. Mater Chem. A. 2018, 6, 7693.

40. Kolodziejski, W.; Zicovich-Wilson, C.; Corell, C.; Perez-Pariente, J.; Corma, A. 27Al and 29Si MAS NMR Study of Zeolite MCM-22. J. Phys. Chem. 1995, 99, 7002.

41. Camblor, M. A.; Corma, A.; Díaz-Cabañas, M.-J.; Baerlocher, C. Synthesis and Structural Characterization of MWW Type Zeolite ITQ-1, the Pure Silica Analog of MCM-22 and SSZ-25. J. Phys. Chem. B. 1998, 102, 44.

42. Xu, D.; Abdelrahman, O.; Ahn, S. H.; Guefrachi, Y.; Kuznetsov, A.; Ren, L.; Hwang, S.; Khaleel, M.; Al Hassan, S.; Liu, D.; Hong, S. B.; Dauenhauer, P.; Tsapatsis, M. A quantitative study of the structure–activity relationship in hierarchical zeolites using liquid-phase reactions. AIChE J. 2019, 65, 1067.

43. Liu, D.; Zhang, X.; Bhan, A.; Tsapatsis, M. Activity and selectivity differences of external Brønsted acid sites of single-unit-cell thick and conventional MFI and MWW zeolites. Micropor. Mesopor. Mat. 2014, 200, 287.

44. Emdadi, L.; Oh, S. C.; Wu, Y.; Oliaee, S. N.; Diao, Y.; Zhu, G.; Liu, D. The role of external acidity of meso-/microporous zeolites in determining selectivity for acid-catalyzed reactions of benzyl alcohol. J. Catal. 2016, 335, 165.

SYNOPSIS TOC

Vapor-Phase Strategy to Pillaring of Two-Dimensional Zeolite

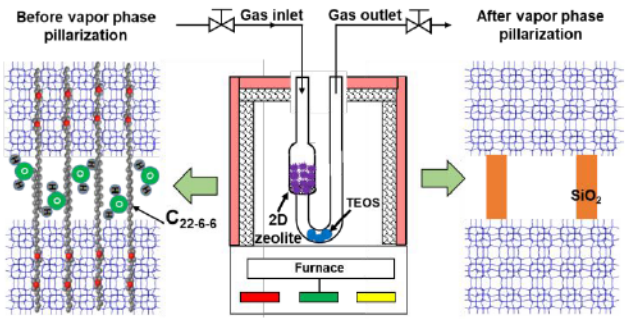

Supporting Information for

Vapor-Phase Strategy to Pillaring of Two-Dimensional Zeolite

Lu Wei[1,2], Kechen Song[2,3], Wei Wu[2], Scott Holdren[4], Guanghui Zhu[5], Emily Shulman[2], Wenjin Shang[6], Huiyong Chen[6], Michael R. Zachariah[4±] and Dongxia Liu[2*]

1. College of Materials Science and Engineering, Beijing University of Technology, Beijing, 100124, China

2. Department of Chemical and Biomolecular Engineering, University of Maryland, College Park, MD, 20742, USA

3. School of Chemical and Environmental Engineering, China University of Mining and Technology, Beijing, 100083, China

4. Department of Chemistry and Biochemistry, University of Maryland, College Park, MD, 20742, USA

5. School of Chemical and Biomolecular Engineering, Georgia Institute of Technology, Atlanta, 30332, USA

6. School of Chemical Engineering, Northwest University, Xi'an, Shanxi, 710069, China

± current address: Department of Chemical and Environmental Engineering, University of California, Riverside mrz@engr.ucr.edu

*Corresponding author:
Prof. Dongxia Liu
Email: liud@umd.edu
Phone: (+1) 301-405-3522
Fax: (+1) 301-405-0523

S1. Experimental

S1.1 Materials

Sodium hydroxide (NaOH, ≥97.0% purity), sulfuric acid (H_2SO_4, 95.0%), and tetraethyl orthosilicate (TEOS, $Si(OC_2H_5)_4$, 98% purity) were supplied by Alfa Aesar. Aluminum sulfate hydrate ($Al_2(SO_4)_3 \cdot 16H_2O$, 98.0-103.0%), benzyl alcohol (99.95% purity) and mesitylene (99% purity) were purchased from Sigma-Aldrich. Deionized (DI) water was used throughout the synthesis. Diquaternary ammonium surfactant ($[C_{22}H_{45}\text{-}N^+(CH_3)_2\text{-}C_6H_{12}\text{-}N^+(CH_3)_2\text{-}C_6H_{13}]Br_2$, ($C_{22\text{-}6\text{-}6}$)) was synthesized following the procedure reported by Ryoo et al[1]. We have explained the procedure in our previous publications[2,3]. The conventional MFI zeolite was purchased from Zeolyst (Si/Al = 80, CBV 8014) in the NH_4^+-form.

S1.2 Synthesis of multilamellar MFI (M-MFI(P) and M-MFI) zeolites

The pillared MFI (PMFI) zeolite was synthesized from the multilamellar MFI that was used as the precursor of PMFI (denoted as M-MFI (P)). The synthesis of M-MFI(P) was conducted following the reported method[1]. In a typical synthesis, a basic solution was obtained by dissolving 0.7 g NaOH in 3.1 g DI water. The basic solution was added dropwise to an acidic solution that was prepared by dissolving 0.4 g H_2SO_4 in 4.2 g DI water under vigorous stirring. After cooling the mixed solution to room temperature, 0.2 g $Al_2(SO)_4 \cdot 16H_2O$ was dissolved in the solution under sonication. Then, 6.3 g TEOS were added and the mixture was stirred magnetically at ambient temperature for 20 h. Finally, the $C_{22\text{-}6\text{-}6}$ solution that was prepared by dissolving 2.2 g $C_{22\text{-}6\text{-}6}$ in 15.0 g DI water at 333 K was added. The resultant mixture was stirred for 2 h before it was transferred into a 45 mL Teflon-lined stainless steel autoclave. The autoclave was kept at 423 K in a convective oven (Yamato DKN400) for 5 days under tumbling at a speed of 40 rpm to hydrothermally synthesize M-MFI(P). The zeolite product was collected by centrifugation, washed with DI water to reduce the pH to ~ 9, and dried in the convective oven at 343 K for 12 h. Afterwards, a portion of the M-MFI(P) sample was calcined at 723 K under N_2 flow (1.67 mL s^{-1}) for 6 h and finally at 823 K under air flow (1.67 mL s^{-1}) for 12 h (temperature ramp rate of 0.033 K s^{-1}) in a furnace (Linderberg Blu M, BF51866A-1) to produce M-MFI zeolite. The rest of the M-MFI(P) sample was used for synthesis of PMFI in the VPP process described below.

S1.3 Synthesis of PMFI zeolite

Two VPP processes were developed to synthesize PMFI zeolites: the first one used two apparatuses (autoclave and furnace) and discrete operation for three steps (TEOS intercalation, TEOS hydrolysis and calcination) (Figure 1), and the second one only used one apparatus (furnace) and one-time continuous operation for three synthesis steps (Figure 3). In the first VPP process, 0.1 g M-MFI(P) sample was placed in a glass vial (5 mL), and then kept in a Teflon cup (50 mL) enclosed in the stainless-steel autoclave. 0.05 g TEOS was added into the Teflon cup and stayed outside of the glass vial. The autoclave was then placed in a convective oven that was preheated to 423 K for 24 h. In the next step, the autoclave was cooled down to ambient temperature in the fume hood, and the glass vial containing the zeolite sample was moved into a new autoclave that contained 1.0 g DI water in the Teflon cup. After heating the autoclave in the same oven at 353 K for 24 h, the zeolite sample was transferred into a crucible

in the furnace (Linderberg Blu M, BF51866A-1). Finally, the sample was calcined following the same procedure as that of M-MFI synthesis in Section 1.2 to form PMFI zeolite.

For the second VPP process for synthesis of PMFI, the "U"-shaped quartz reactor was used as a container for holding the zeolite sample. The outer diameter of quartz tube is 1/4" and the "bulb" region is 1/2" in the reactor. Typically, 0.1 g M-MFI(P) sample was loaded into one side of the "U"-shape reactor, and 0.05 g TEOS was dropped into the reactor from the other side. A quartz frit separated the zeolite sample from direct contact with TEOS liquid in the reactor. The reactor was then placed into the furnace and connected in the gas flow lines according to the schematics in Figure 3. After running the furnace according to the temperature profile and gas flows in Figure 3, the reactor was cooled down to ambient temperature and PMFI was taken out for physiochemical property characterizations.

S1.4 Material characterization

X-ray diffraction (XRD) analysis was done on a Rigaku Rotaflex Diffractometer using Cu K_α radiation (λ = 1.5418 Å). N_2 adsorption-desorption isotherm was measured on an Autosorb-iQ analyzer (Quantachrome Instruments) at 87 K. The sample was degassed for 12 h at 573 K before the isotherm measurement. Scanning electron microscopy (SEM) was performed with Hitachi Model SU-70. Transmission electron microscopy (TEM) was obtained using a JEM 2100 LaB6 electron microscope operating at 200 kV. Fourier transform infrared (FTIR) spectra of zeolite and pyridine adsorbed on zeolite samples were recorded using a (FTIR) spectrometer (Nicolet Magna-IR 560) with a resolution of 2 cm^{-1}. Elemental composition of the zeolite samples was determined by inductively coupled plasma optical emission spectroscopy (ICP-OES, PerkinElmer, Optima 7000DV). Solid-state magic-angle spinning (MAS) nuclear magnetic resonance (NMR) spectra were recorded on a Bruker Avance AV 500. ^{29}Si MAS NMR spectra were recorded at 99.37 MHz using 4 mm rotors at a spinning speed of 8 kHz, a dwell time of 16.65 μs, a $\pi/2$ pulse of 4.0 μs and a recycle delay of 60 s. The spectra were referenced with respect to 3-(trimethysilyl)-1-propanesulfonic acid salt. ^{27}Al MAS NMR spectra were recorded at 130.34 MHz using 4 mm rotors at 14 kHz spinning speed, a dwell time of 0.5 μs, a selective $\pi/18$ pulse of 0.3 μs and a recycle delay of 0.1 s. An aqueous solution of $Al_2(SO_4)_3$ (0.1 M) was used as reference. The amount of water and organics in the zeolite samples was measured using a thermo-gravimetric analyzer (TGA) (Shimadzu, TGA-50). In the TGA measurement, the temperature was increased to 1273 K under flowing air (0.833 mL s^{-1}, breathing grade, Airgas) at a ramp rate of 0.167 K s^{-1}.

S1.5 Catalysis tests

All the zeolite samples were first transformed into H^+-form before the catalysis tests. The calcined sample was dispersed in 1.0 M aqueous NH_4NO_3 solution (weight ratio of zeolite to NH_4NO_3 solution = 1:10) for 3 h at 353 K. The sample was collected by centrifugation and washed with DI water. The process was repeated three times, then the zeolite sample was dried in a convective oven at 343 K for 12 h. The zeolite in NH_4^+-form was treated in air (1.67 mL s^{-1}, breathing grade, Airgas) in a furnace by increasing the temperature from ambient to 823 K at 0.167 K s^{-1} rate and holding at this temperature for 4 h.

The liquid phase catalytic conversion of benzyl alcohol in mesitylene was carried out in a three-necked round bottom flask (100 mL) equipped with a reflux condenser and heated in

a temperature controlled oil bath under atmospheric pressure and magnetic stirring (500 rpm stirring speed) conditions. Experimental details and product analyses have been reported in our previous publications[4-5].

S2. Results and discussion

S2.1 Effect of TEOS quantity on formation of PMFI in VPP process

To examine the effect of TEOS quantity on PMFI formation, the mass of TEOS was varied from 0.375 g, 0.100 g, 0.05 g, 0.01 g and 0.005 g, in the intercalation step. The mass of the M-MFI(P) sample was kept at 0.100 g for these experiments. The mass ratios of TEOS/M-MFI(P) were calculated to be 3.75, 1.00, 0.50, 0.10 and 0.05. Figure S1 shows the morphology of M-MFI(P) samples after TEOS intercalation. The wetness of the samples decreases with decreasing TEOS/M-MFI(P) ratios. In particular, the sample looked like dry powder when the TEOS/M-MFI(P) ratio was below 0.5. The Si/Al ratios in Table S2 indicate that nearly all the TEOS was moved into the zeolite to form PMFI except the one TEOS/M-MFI(P) ratio of 3.75. Figures S2 and S3 show the XRD patterns and N_2 isotherms as well as pore size distribution of these PMFI samples.

Figure S1. Bulk morphology of M-MFI(P) after TEOS intercalation in the VPP process. The mass ratio of TEOS/M-MFI(P) was controlled to (1) 3.75, (2) 1.00, (3) 0.50, (4) 0.10 and (5) 0.05, respectively. The numbers in the label of each glass vial is TEOS mass (unit: gram). (synthesis conditions: 343 K, M-MFI(P) = 0.1 g and mass ratio of H_2O/M-MFI(P) = 10 in the hydrolysis step)

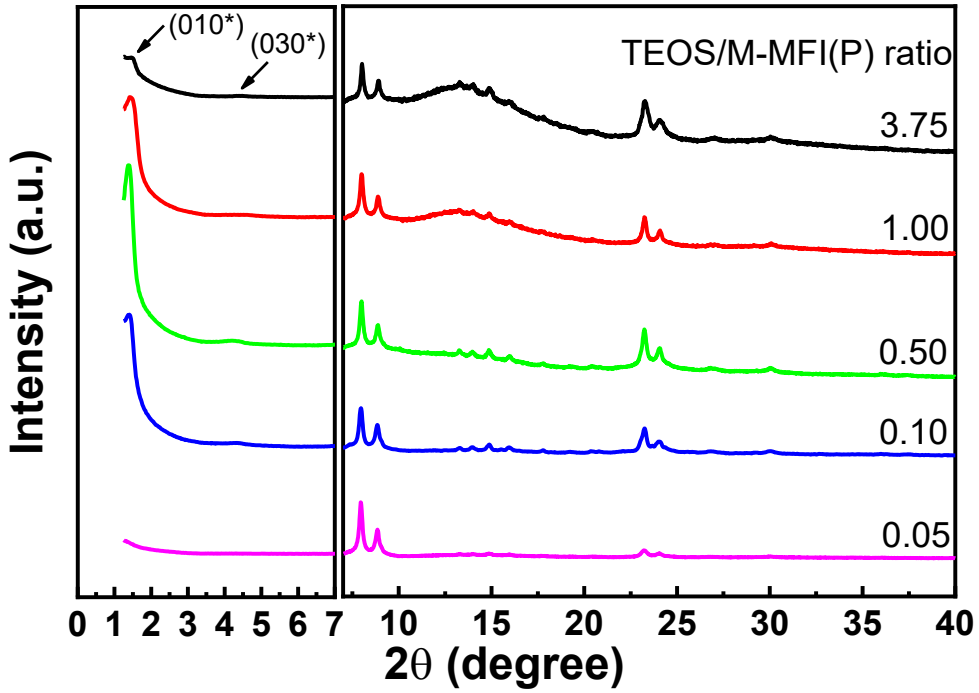

Figure S2. XRD patterns of PMFI synthesized with different TEOS amount (represented by TEOS/M-MFI(P) ratio) added in the TEOS intercalation step in the VPP process.

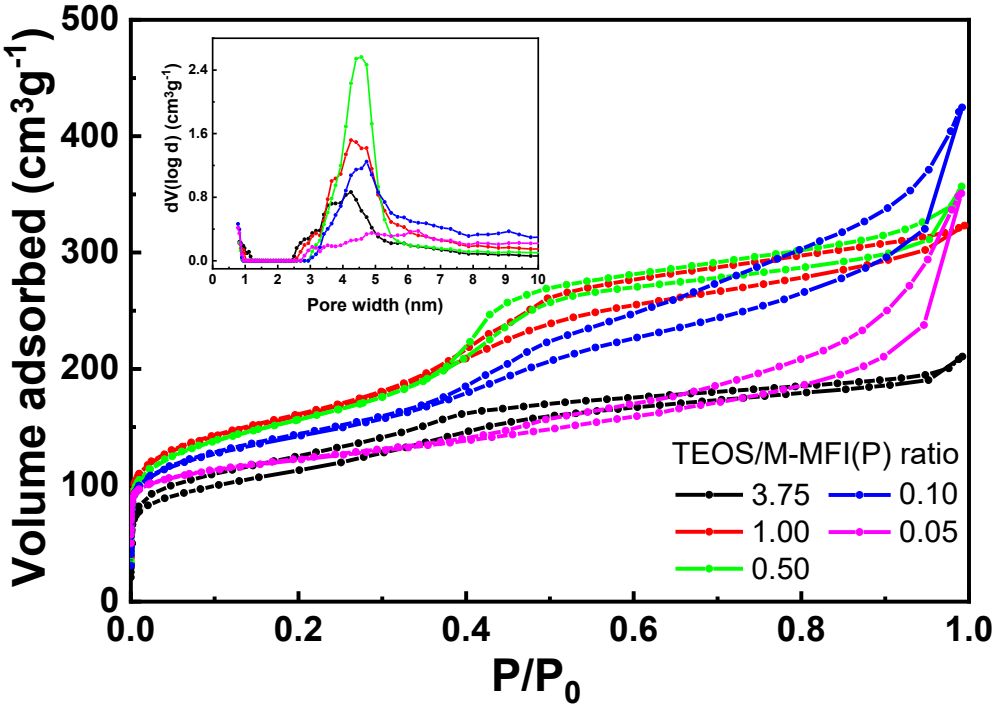

Figure S3. N_2 isotherms and NLDFT pore size distributions of PMFI synthesized with different TEOS amount (represented by TEOS/M-MFI(P) ratio) added in the TEOS intercalation step in the VPP process.

Table S1. Textural properties of PMFI synthesized under different ratio of TEOS/multilamellar MFI.

TEOS/M-MFI(P) ratio	V_{micro} [a] [$cm^3\ g^{-1}$]	S_{micro} [a] [$m^2\ g^{-1}$]	S_{ext} [a] [$m^2\ g^{-1}$]	V_{total} [b] [$cm^3\ g^{-1}$]	V_{meso} [c] [$cm^3\ g^{-1}$]	S_{BET} [d] [$m^2\ g^{-1}$]
3.75	0.012	47	324	0.294	0.282	371
1.00	0.054	87	442	0.467	0.413	529
0.50	0.099	133	484	0.526	0.430	617
0.10	0.106	140	419	0.526	0.420	559
0.05	0.103	245	194	0.367	0.264	439
M-MFI [e]	0.087	196	253	0.371	0.284	448

[a] Determined from t-plot method; [b] Determined by non-localized density functional theory (NLDFT) method from adsorption branch of N_2 isotherm; [c] $V_{meso} = V_t - V_{micro}$; [d] Determined from Brunauer, Emmett, and Teller (BET) method; [e] Reported in our previous publication[2].

Table S2. Si and Al compositions of PMFI zeolites synthesized with different TEOS/M-MFI(P) ratios in the VPP process.

PMFI [a] (composition)	TEOS/M-MFI(P) ratio				
	3.75	1.00	0.50	0.10	0.05
Si/Al ratio [b]	142	74	61	51	50
Si/Al ratio [c]	111	70	61	53	50

[a] All PMFI samples were prepared from M-MFI(P) (Si/Al ratio=49); [b] Calculated from Si and Al contents in M-MFI(P) and TEOS used in VPP process; [b] Determined by elemental analysis (ICP-OES).

S2.2 Effect of TEOS intercalation temperature on formation of PMFI in VPP

To study the influence of TEOS intercalation temperature on formation of PMFI in the VPP process, the temperature was varied from 363 K, 383 K, 403 K to 423 K, in sequence. The XRD data in Figure S4 show that all four PMFI samples synthesized at different intercalation temperatures have similar diffraction patterns. The appearance of both wide-angle and low-angle XRD peaks indicate that both MFI crystalline structure and long-range ordering of zeolitic layers are preserved in the VPP process. The PMFI structure does not seem to be dependent on the intercalation temperature in the studied temperature range. The similar N_2 uptake and pore size distribution in the isotherm data in Figure S5 further confirm this conclusion.

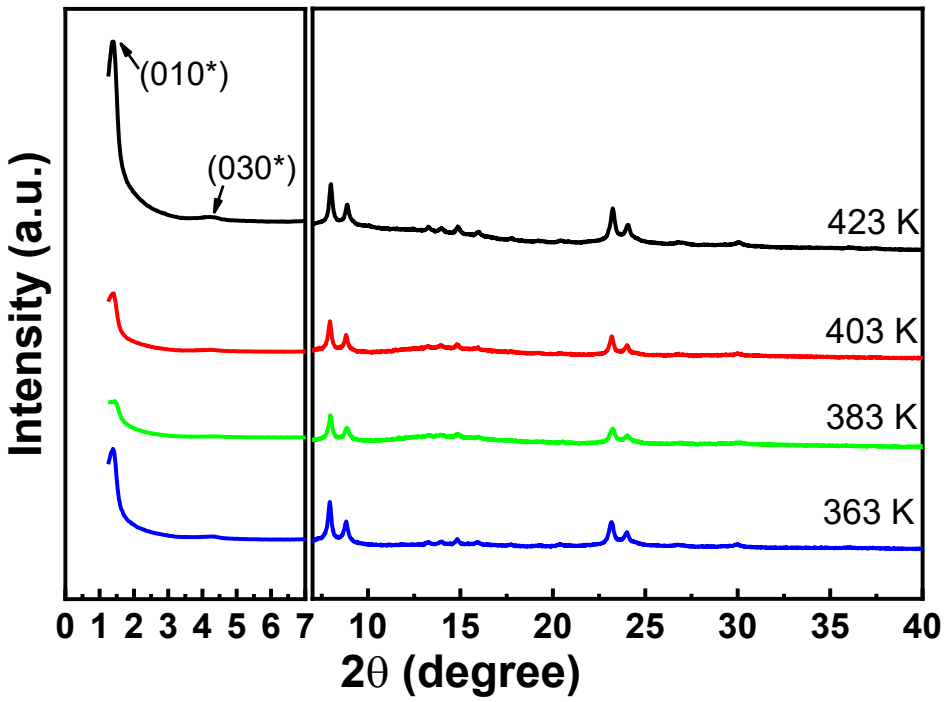

Figure S4. XRD patterns of PMFI synthesized at different TEOS intercalation temperatures in the VPP process.

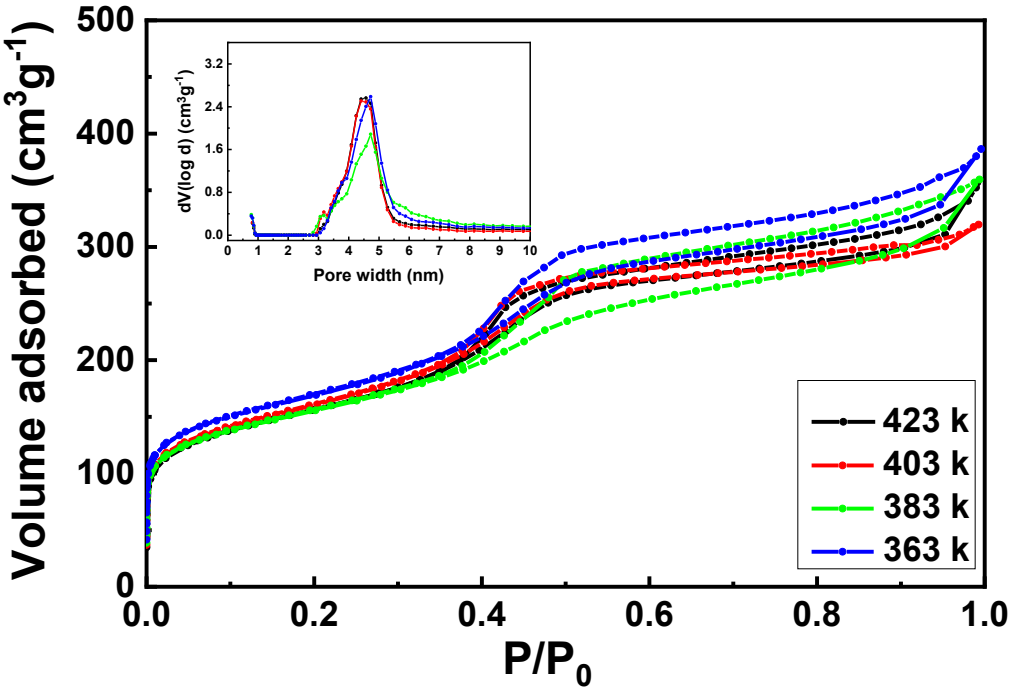

Figure S5. N_2 isotherms and NLDFT pore size distributions of PMFI synthesized at different TEOS intercalation temperatures in the VPP process.

S2.3 Effect of water amount in hydrolysis step on formation of PMFI in VPP

In the hydrolysis step, water quantity was varied from 0.0 g, 0.1 g, 0.5 g and 1.0 g. The rest of the synthesis procedure was the same as that described in Section S1.3. Figures S6 and S7 confirm that water does not influence the crystallinity and textural properties of the synthesized PMFI zeolite significantly, since all four samples had similar XRD patterns and N_2 isotherms.

Water content in M-MFI(P) was quantified byTGA measurement. As shown in Figure S8, the $C_{22\text{-}6\text{-}6}$ template started to lose weight at 483 K, and the decomposition was completed at ~900 K. The initial weight loss should be due to water desorption, and the final weight loss was caused by $C_{22\text{-}6\text{-}6}$ combustion. According to TGA data of $C_{22\text{-}6\text{-}6}$, the first weight loss (< 563 K) in M-MFI(P) was attributed to the removal of adsorbed water. The higher weight loss in M-MFI(P) (dried in convective oven) than M-MFI(P) (dried by vacuum oven) at this temperature range indicates higher water content in the former sample. The calculation shows that ~16 wt% H_2O adsorbed in M-MFI(P) dried regularly in the convective oven. After vacuum drying, the remaining water in M-MFI(P) was ~12 wt%.

The following calculation shows the correlation between water adsorbed in M-MFI(P) and TEOS hydrolysis. For 0.1 g M-MFI(P), the adsorbed water in zeolite is 0.1 g x 16 wt% = 0.016 g, equivalent to 8.88 x 10^{-4} mol H_2O. According to the reaction stoichiometry, 4 H_2O + 1 $Si(OC_2H_6)_4$ → $Si(OH)_4$ + 4 C_2H_6OH, 3.55 x 10^{-3} mol TEOS can be hydrolyzed, equivalent to ~0.05 g TEOS amount. Therefore, water adsorbed in M-MFI(P) zeolite is sufficient for hydrolysis of TEOS used in PMFI synthesis with TEOS/M-MFI(P) < 0.5. This is consistent with our experiment results that PMFI could be successfully synthesized with zero water addition in the hydrolysis step. For comparison, the M-MFI(P) sample was dried in a vacuum oven at 393 K for 12 h, and the pillaring structure in PFMI did not form, as shown by the absence of clear low-angle XRD peaks in Figure S9.

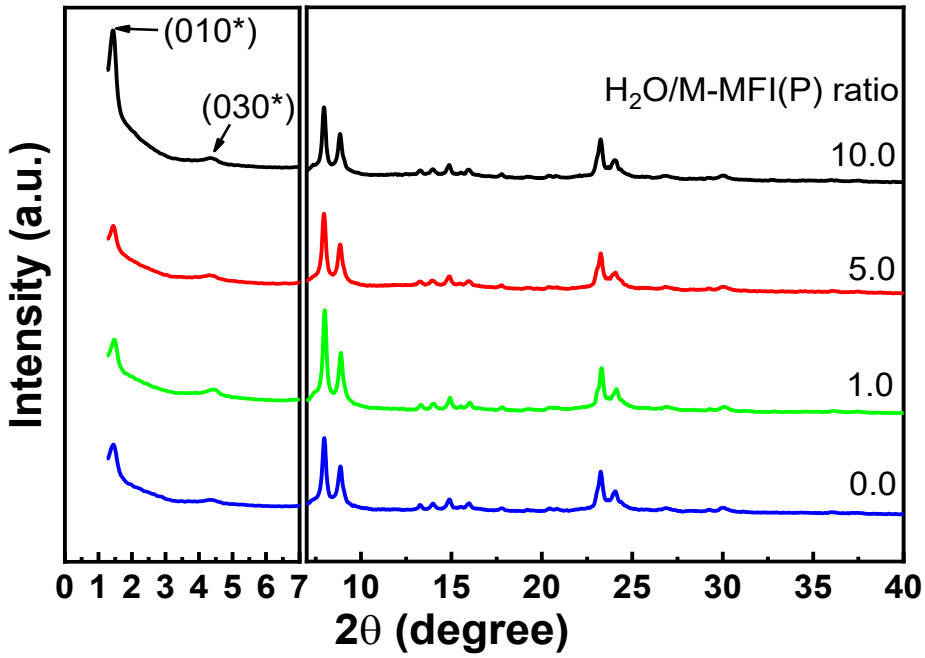

Figure S6. XRD patterns of PMFI synthesized with different water amount (represented by H_2O/M-MFI(P) ratio) loaded in the TEOS hydrolysis step in the VPP process.

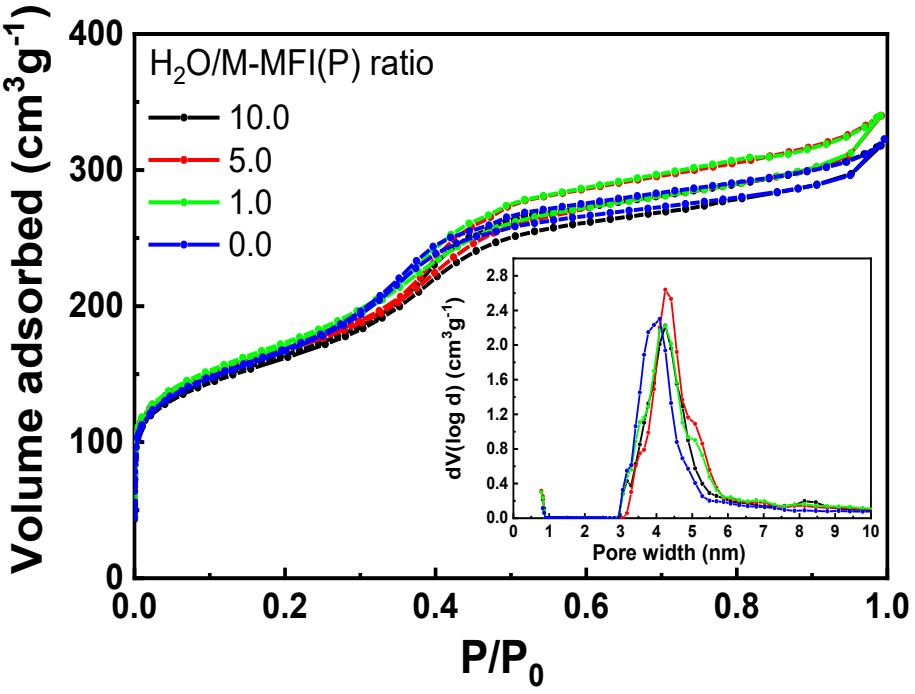

Figure S7. N_2 isotherms and NLDFT pore size distributions of PMFI synthesized with different water amount (represented by H_2O/M-MFI(P) ratio) loaded in the TEOS hydrolysis step in the VPP process.

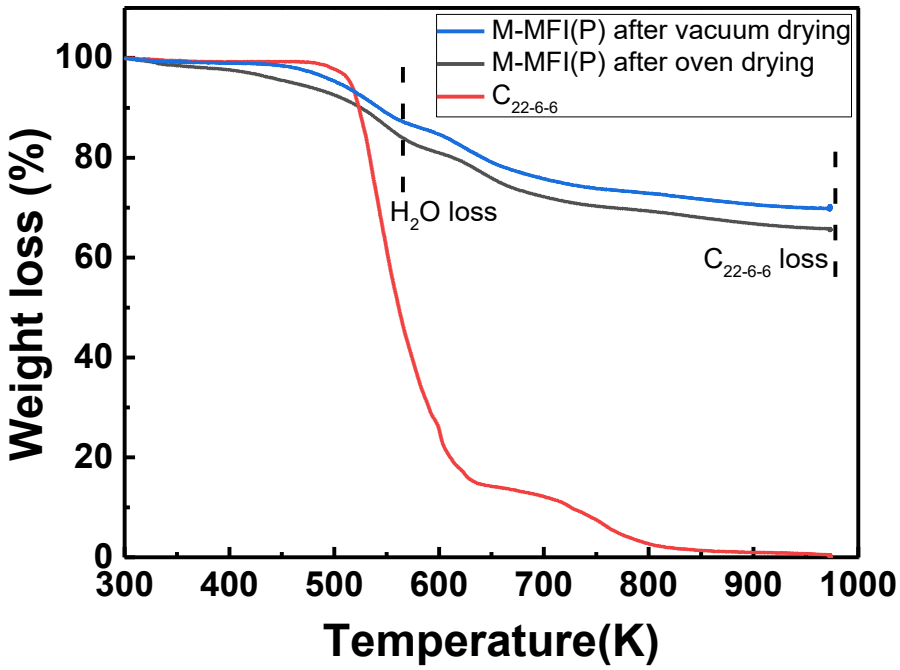

Figure S8. TGA of M-MFI(P) dried in a convective oven at 343 K for 12 h and with M-MFI(P) pre-dried at 393 K for 12 h in vacuum oven, respectively. $C_{22\text{-}6\text{-}6}$ template used in M-MFI(P) synthesis was included for comparison.

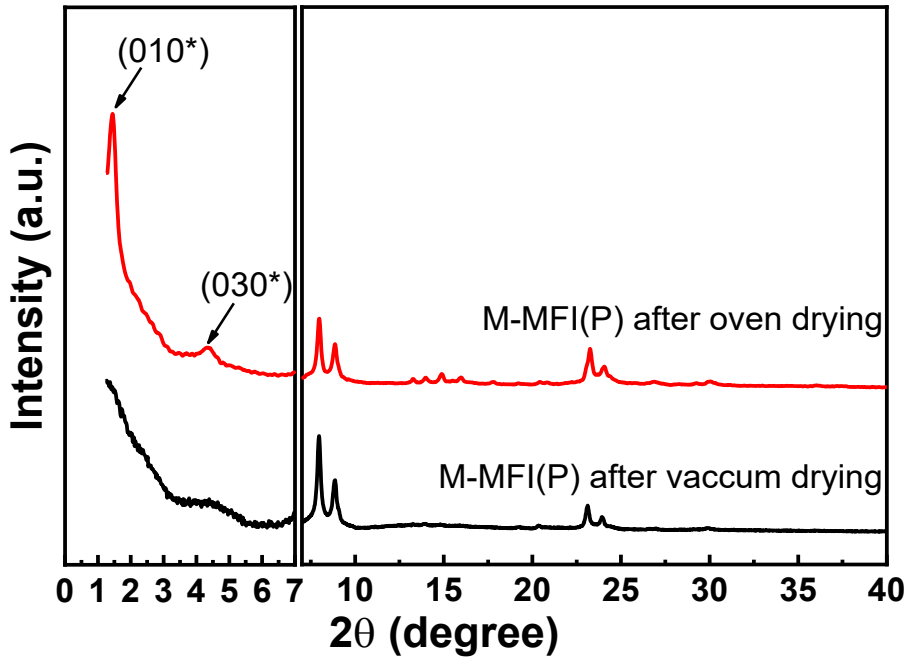

Figure S9. XRD patterns of PMFI zeolites prepared in VPP process with M-MFI(P) dried in a convective oven at 343 K for 12 h and with M-MFI(P) pre-dried in vacuum oven at 393 K for 12 h, respectively, before TEOS intercalation.

S2.4 Characterization of PMFI prepared by one-unit under one-time VPP operation

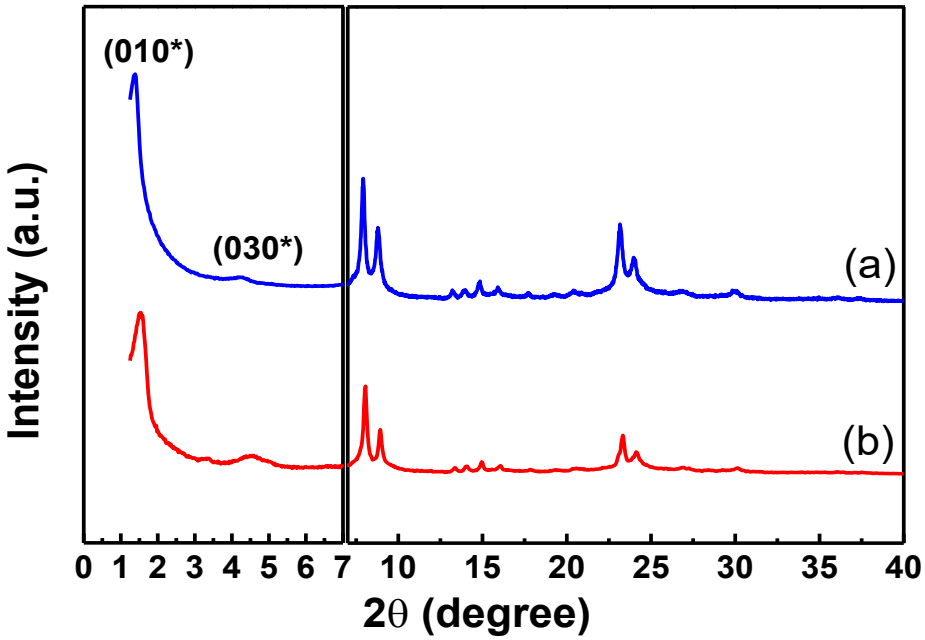

Figure S10. XRD data of PMFI prepared by the VPP process using (a) the multiple-step operation (scheme shown in Figure 1) and (b) one-unit under one-time operation (scheme shown in Figure 3), respectively.

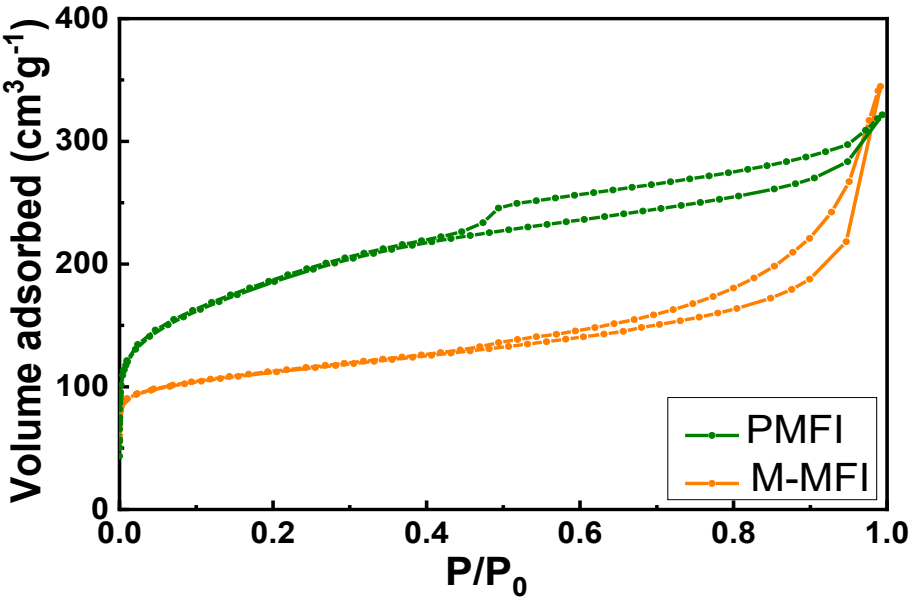

Figure S11. N_2 isotherm of PMFI prepared by the VPP process using the one-unit under one-time operation (scheme shown in Figure 3). The N_2 isotherm of M-MFI was represented here for comparison purpose.

S2.5 Catalytic performances of PMFI samples prepared by VPP and liquid-phase pillarization

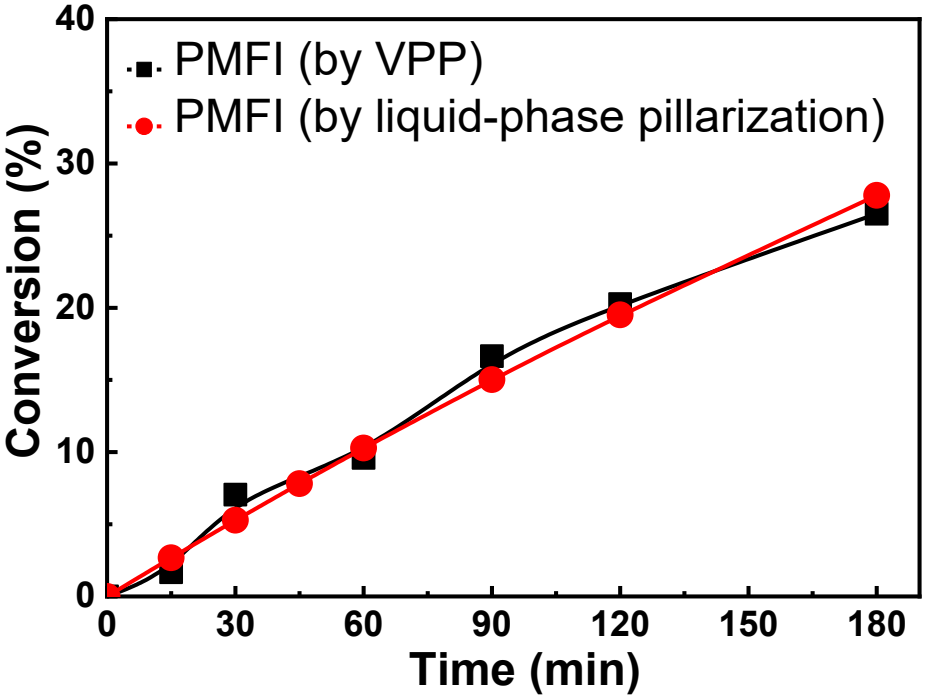

Figure S12. Benzyl alcohol conversion in mesitylene over PMFI samples prepared by both the VPP and the conventional liquid-phase pillarization, respectively. (Reaction condition: 348 K, 0.075 g catalyst, 500 rpm stirring speed.)

References

1. Choi, M.; Na, K.; Kim, J.; Sakamoto, Y.; Terasaki, O.; Ryoo, R. Stable single-unit-cell nanosheets of zeolite MFI as active and long-lived catalysts. Nature 2009, 461, 246.

2. Emdadi, L.; Wu, Y.; Zhu, G.; Chang, C. C.; Wei, F.; Pham, T.; Lobo, R, F.; Liu, D. Dual template synthesis of meso- and microporous mfi zeolite nanosheet assemblies with tailored activity in catalytic reactions. Chem. Mater. 2012, 26, 1345.

3. Liu, D.; Bhan, A.; Tsapatsis, M.; Hashimi, S. A. Catalytic Behavior of Brønsted Acid Sites in MWW and MFI Zeolites with Dual Meso- and Microporosity. ACS. Catal. 2011, 1, 7.

4. Zhang, X.; Liu, D.; Xu, D. Asahina, S.; Cychosz, K. A.; Agrawal, K. V. Synthesis of self-pillared zeolite nanosheets by repetitive branching. Science 2012, 29, 1684.

5. Liu, D.; Zhang, X.; Bhan, A.; Tsapatsis, M. Activity and selectivity differences of external Brønsted acid sites of single-unit-cell thick and conventional MFI and MWW zeolites. Micropor. Mesopor. Mater. 2014, 200, 287.